PROPAGATION OF SHOCK WAVES IN POLYTROPIC GAS SPHERES

D.K. Nadezhin and D.A. Frahk-Kamenetskiy

(NASA-TT-F-14438) PROPAGATION OF SHOCK WAVES IN POLYTROPIC GAS SPHERES D.K. Nadezhin, et al (NASA) Jun. 1972 41 p CSCL 20D G3/12

N72-32315

Unclas 43360

Translation of "Dvizheniye udarnykh voln v politropnykh gazovykh sharakh", Voprosy kosmogonii, Vol. 10, 1964, pp.154-178.

Reproduced by
NATIONAL TECHNICAL INFORMATION SERVICE
U S Department of Commerce
Springfield VA 22151

NATIONAL AERONAUTICS AND SPACE ADMINISTRATION
WASHINGTON, D.C. 20546 JUNE 1972

41 pg.

Propagation of shock waves in polytropic gas spheres

PROPAGATION OF SHOCK WAVES IN POLYTROPIC GAS SPHERES

NADEZHIN D.K.; D.A. FRANK-KAMENETSKIY

The propagation of shock waves in polytropic gas spheres was investigated in this work. The partial differential equations describing spherically symmetrical adiabatic motions of an ideal gas are integrated using a method of finite differences. The adiabatic index is taken as equal to 5/3. Stationary models (polytropies with n indices equal to 1.5 and 3.0) were perturbed in the following way: an inward velocity was given to the matter located near the center (central collapse), then the collapse was produced in some peripheral layer, and finally the cooling of the central star region. All these perturbations have lead the formation of shock waves. Upon passage of this wave on the surface of the star, a fraction of the stellar matter would aquire a speed exceeding the parabolic one leading to the formation of an envelope.

The envelope has a steep velocity gradient: the envelope density falls off exponentially with an increasing distance from the centre of the star.

A set of calculations was performed as a function of the strength of perturbation. The strongest pertur-

bations have lead to the total star disintegration and the weakest one to the expulsion of about 10^{-6} of total mass. The calculations permit the evaluation of a relation between the kinetic energy expanding envelope and its mass. This relation can be well approximated by a power function and but slightly depends on the perturbation shape. The last property permits its application for the masses of Novae. For the fast Novae of NAgl 1918 and NPer 1901 types, the masses are computed to be of the order of several solar masses and for the slow Novae of NAur 1891 and NHer 1934 types of the order of 0.2 - 0.02 $M_{\odot}$. After the escape of shock waves and formation of an envelope, the bulk mass of the star is pulsating with a frequency approximated by the principal mode given by the linear pulsation theory.

The basic results of the calculations are given in tables and figures.

INTRODUCTION

At present the high-speed computing machines are utilized more and more in astrophysical investigations. As an example, the most interesting results, pertaining to the internal structure and evolution of stars, have been obtained during the last years using these machines. At present one of the basic problems of the theory of star evolution is the transformation of quasi-stationary evolution to such basically non-stationary processes as the stellar pulsation and the bursts of Novae and Super-Novae. However, this problem is very complicated and is difficult to investigate. Therefore it is reasonable to try first the investigation of basically non-strationary processes neglecting the transition.

At present a great deel of time is given to the study of propagation of shock waves in a medium of variable density (1, 2), and, as a result of the study, the shock wave theory of the bursts of Novae and Super-Novae is relatively well advanced (1).

Until present this study has been conducted using the approximate or semi-approximate methods. The application of high-speed machines considerably increases the study range of this most interesting phenomenon. Careful combination of the precision present in machine computations

with the approximate investigations should lead to the final answer pertaining to the nature of Novae and Super-Novae bursts.

Because this problem is a complex one, the first steps are only concerned with an investigation of rough models. In the present work the results of calculations by a fictitious viscocity method, with respect to the adibatic propagation of strong shock waves in spherically-symmetric polytropic models of stars, are given. The process of the arrival of a shock wave on the star surface initiates the bursts of Novae and Super-Novae.

§1. EQUATIONS OF PROPAGATION

The Lagrange form for the description of the equations of motion is utilized in this work. At spherically-symmetrical gas motions, the mass m contained inside of a sphere of r radius can be taken as one of the Lagrangian coordinates. All the physical values will be the functions of time t and of coordinate m.

The equations describing the spherically-symmetrical motion of an ideal gas with radiation are:

$$\left.\begin{aligned} \frac{\partial r}{\partial t} &= u; \\ \frac{\partial u}{\partial t} &= -4\pi r^2 \frac{\partial P}{\partial m} - \frac{Gm}{r^2}; \\ \frac{\partial E}{\partial t} &= -P\frac{\partial V}{\partial t} + 16\pi^2 \frac{\partial}{\partial m}\left[\frac{Kr^4}{V}\frac{\partial T}{\partial m}\right] + \varepsilon(V, T); \\ V &= 4\pi r^2 \frac{\partial r}{\partial m}; \\ P &= P_g + P_r = \frac{R}{\mu(m)}\frac{T}{V} + \frac{1}{3}aT^4; \\ E &= \frac{P_g V}{\gamma - 1} + VaT^4. \end{aligned}\right\} \qquad (1)$$

where r is the distance between some gas element and the star center; u is its speed, P is the pressure; Pg is the gas pressure; Pr is the radiation pressure; $V = 1/\rho$ is the specific volume; T is the temperature; E is the internal energy per unit mass; $\mu(m)$ is the molecular weight which for a general case, is a function of the Lagrangian coordinate; ε is the energy discharge per unit mass and per unit time; R is the gas constant; G is the constant of gravitation; a, is the radiation density constant; γ is the ratio of specific heat capacities; and K is the heat conductivity coefficient.

In a case of heat energy transfer by radiation

$$K = \frac{4}{3}\frac{acV}{\varkappa(V, T)}T^3,$$

where C, the speed of light and $\varkappa$ is the opacity.

It is convenient, however, to measure the principal values in the following system of units (an arrow means that "it is measured in units" and 0 index indicates that it is with respect to moment t = 0);

$$
\left.
\begin{aligned}
& r \to R_0 - \text{the star radius at } t = 0; \\
& m \to M_0 - \text{the star mass;} \\
& u \to \sqrt{\frac{GM_0}{R_0}}, \quad t \to R_0 \sqrt{\frac{R_0}{GM_0}}; \\
& P \to \frac{GM_0^2}{4\pi R_0^4}, \quad E \to \frac{GM_0}{R_0}; \\
& T \to \frac{G}{R}\frac{M_0}{R_0}, \quad \rho \to \frac{M_0}{4\pi R_0^3}; \\
& \varkappa \to c\varkappa^2/g \qquad \varepsilon \to \text{Energy/g.S}
\end{aligned}
\right\} \qquad (2)
$$

A system of (1) equations after using a system of units given in (2) will be:

$$
\left.
\begin{aligned}
\frac{\partial r}{\partial t} &= u; \\
\frac{\partial u}{\partial t} &= -r^2 \frac{\partial P}{\partial m} - \frac{m}{r^2}; \\
\frac{\partial E}{\partial t} &= -P\frac{\partial V}{\partial t} + K_1 \frac{\partial}{\partial m}\left[\frac{r^4}{\varkappa}\frac{\partial T^4}{\partial m}\right] + K_2\varepsilon; \\
V &= r^2 \frac{\partial r}{\partial m}; \\
P &= \frac{1}{\mu(m)}\frac{T}{V} + AT^4; \\
E &= \frac{1}{\mu(m)}\frac{T}{\tau - 1} + 3AVT^4,
\end{aligned}
\right\} \qquad (3)
$$

where

$$\left.\begin{aligned} K_1 &= \frac{16\pi^2 ca}{3}\left(\frac{G}{R}\right)^4 \frac{R_0^{7/3} M_0^{7/3}}{G^{7/3}}; \\ K_2 &= \frac{R_0^{7/3}}{G^{7/3} M_0^{7/3}}; \\ A &= \frac{4\pi a G^3}{3R^4} M_0^2. \end{aligned}\right\} \qquad (4)$$

In concrete solutions of a system (3) it is necessary to have the initial and boundary conditions. Later on we will study only the adiabatic motions ($K_1 = K_2 = 0$). For a case of adiabatic motions the boundary conditions are:

$$r = 0,\ u = 0 \quad \text{at} \quad m = 0; \qquad (5a)$$

$$P = AT^{1/2} \quad \text{at} \quad m = 1. \qquad (5b)$$

The first condition signifies that gas fills in the whole star volume up to its centre and that the gas particles are motionless in the centre. The second condition signifies that the pressure at the star surface is equal to the radiation pressure.

Let us take the following initial conditions:

$$\left.\begin{aligned} u|_{t=0} &= \varphi(m); & r|_{t=0} &= r_n(m); \\ P|_{t=0} &= P_{c0}[\theta_n(m)]^{n+1}; & \rho|_{t=0} &= \rho_{c0}[\theta_n(m)]^n. \end{aligned}\right\} \qquad (6)$$

where n is the polytropic index; $\theta_n(m)$, the Len-Emden function of n index; $r_n(m)$, the balanced radius of a sphere of mass m; P_{co} and ρ_{co} are the values of pressure and density respectively, at the e star centre prior to the initiation of a non-stationary process; $\varphi(m)$ is the arbitrarily-given perturbation which takes the star out of its equilibrium state. In such a manner a problem of adiabatic, spherically-symmetrical gas motions in polytropic gas/spheres has been solved. In computing, the molecular weight μ was considered to be constant within the star. The computations have been made for two polytropic cases with the indexes (n) equal to 1.5 (convective model) and 3.0 (standard model) where the radiation pressure was not taken into consideration in the convective model (A=0) and was assumed to be of the following nature in the standard model:

$$\mu^4 A = 1{,}00. \qquad (7)$$

In the process of computation the temperature was taken with respect to the unit of molecular weight; $T_1 = T/\mu$, and under these conditions, as it is easy to see, a system (3) contains only one constant which depends of the star mass: $\mu^4 A$. If the radiation pressure can be

neglected, so a system of equation (3) and, also the initial and boundary conditions contain no constants which are the functions of star mass and its radius(dimensionless central density P_{co} and pressure P_{co} are only the functions of a polytropic index $\underline{n}$) and, therefore, for the same the gas motions in polytropic gas spheres with the same polytropic index $\underline{n}$ are similar. The similarity signifies that a single solution of dimensionless system (3) for any arbitrary value of M_o and R_o leads to a solution of dimensional system (1) by means of stretching the spatial and temporary coordinate and by multiplying a constant multiplier.

In evaluating the radiation pressures, the similitude with respect to a radius $\underline{R_o}$ is conserved but it is not conserved with respect to the star mass. However, if the value of $\mu^2 M_o/M_\odot$ does not exceed 3 - 5, so the parameter β, which is the ratio of gas pressure to the total pressure does not significantly deviates from 1 and is slightly affected by M_o(3). Therefore adiabatic gas motions in stars of relatively small mass, constructed according to a standard model, can be also considered as approximately-similar with respect to the star mass. In our case the value of $\mu\sqrt[4]{1} = 1$ parameters corresponds to $\beta = 0{,}9954$.

A system of equations (3) with boundary (5) and initial (6) conditions has been numerically integrated using a high-speed computing machine and where in all the cases the adiabatic index γ was taken as equal to 5/3.

§ 2. COMPUTATION METHOD

System (3) is not suitable for the numerical integration, therefore it was somewhat modified.

In the first place, a new Lagrangian coordinate j was introduced instead of the Lagrangian coordinate m by means of a functional relation $m = m(j)$. In this connection an operator $\partial/\partial m$ in (3) is replaced with $\frac{1}{m_j'}\frac{\partial}{\partial j}$. The purpose of such substitution is to be able to approximate with equal precision both the internal and external layers at an uniform subdivision of the Lagrangian coordinate into calculational intervals. Such replacement was applied in (4) for the calculation of star evaluation.

In the second place, the shock waves are formed in the motion process. To evaluate these waves, a fictitious viscosity method, by which the (P + 9) value is substituted into the second and the third equations of (3) system in place of P pressure, is utilized, where q is the fictitious viscosity proportional to the square of a velocity gradient (5). The fictitious viscosity practically is not equal zero only on a front of the shock wave. Here it is distributed over the space containing a few calculating

points. In this connection, the Huygens conditions are automatically fulfilled at the passage of gas through the front of the shock wave. The gas motion on the both front sides remains adiabatic.

M(j) function can be given arbitrarily. In particular, it may be selected in such a manner that j will coincide with radius of a sphere containing m mass at the time t = 0. In calculating, the j has been selected to be proportional to the balanced radius and a coefficient of the proportionality has been selected in such a manner as to have integral values for j at the distribution points.

For numerical integration a system of the partial differential equation (3) was approximated by a system of the algebraic difference equations. The methods of substitution of the differential equations with the different equations are described in detail in (4, 5, 6). A method of the integer and semi-integer points was used for the more precise approximation. The whole star from its centre to its surface was subdivided along the Langrangian coordinates into 101 "integral" and 101 "semi-integral" points. A radius r and velocity u were evaluated at the "integral" points whereas such thermodynamic values as pressure, density, and temperature were evaluated at the "semi-integral" points. Since the surface boundary condition is given as a pressure

C

it is convenient to select j in such a manner as to have a "semi-integral" to correspond to the surface.

j = 0 corresponds to a centre of the star and j = J+ 1/2 is at the surface; J is the integer equal 100 for our case. Here we are not writing out the difference equations because they are analogous with those given in a book by Rikhtmayyer (5). A system of the different equations was solved using an obvious scheme and the calculations were made with variable steps with respect to time. The machine was selecting the maximum possible step corresponding to the first and the second courant conditions. The balance polytropic models present in the initial conditions given in (b) were preliminary evaluated using a machine. The Len-Emden differential equations were integrated using the Runge-Kutta method and the tables of the Len-Emden functions found to be very helpful.(7).

§3. PERTURBATIONS

A perturbation function $\varphi(m)$ was given in two aspects shown in figures 1a and 1b.

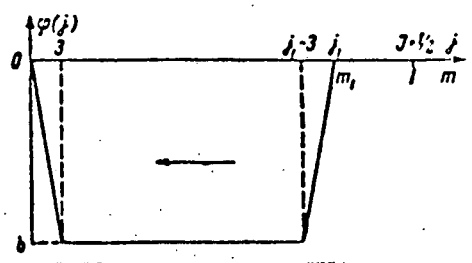

Figure 1a. Central Collapse

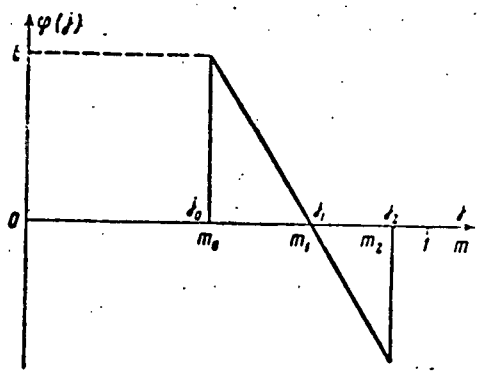

Figure 1b. Collapse of the Surface Layers

For the first case, some region located near the star centre (the positive sign of $\varphi(m)$ corresponds to the motion directed from the centre to the surface) is pertrubed. All the points with the Lagrangian coordinates less than m_1 are given a velocity directed toward the centre.

A velocity amplitude, and m, a mass, are the variable parameters where m is a subject of perturbation. For the second case, the collapse of gas masses in the intermediate layers takes place. The central explosion is imitated in the first case and the under surface explosion in the first case and the under surface explosion in the second case at m nearing the one. Since the concrete mechanism of the generation of strong shock waves at the Novae bursts is unknown, it is natural to arbitrarily vary the produced perturbations between the largest possible limits. Therefore we have made two additional calculations

with an artificially-cooling centre for a polytropic case where n = 3. At such perturbation, a non-equilibrium model is distinguished from a balanced one by having a lower temperature in some regions located near the centre; the initial velocity $\varphi(m)$ is equal to zero every where; the density and the balanced radius remain the same as in (b), but the pressure in the cooling region is different from the balanced one and leads to the violation of the equation of hydrostatic equilibrium.

§4. SHOCK WAVE PROCESS

At the central perturbation (figure 1a) the gas motion has the following character: the gas is strongly compressed and heated in moving toward the star center (figures 2 and 3); soon a reflected shock wave propagating toward the surface is formed near the centre with a velocity amplitude of the reflected wave approximately two times smaller than that of the perturbation amplitude. This can be explained by the fact that a portion of the perturbation kinetic energy is lost on heating the gas under compression to the centre. We are obtaining the partial imitation of a central explosion with the total discharged energy equal to the kinetic energy of induced perturbation.

In the next moments the shock wave moving toward the surface is slightly quenched at first, and then begins to increase its amplitude after entering the nearest layers where a substantial decrease in density takes place.

(figures 3 and 4).

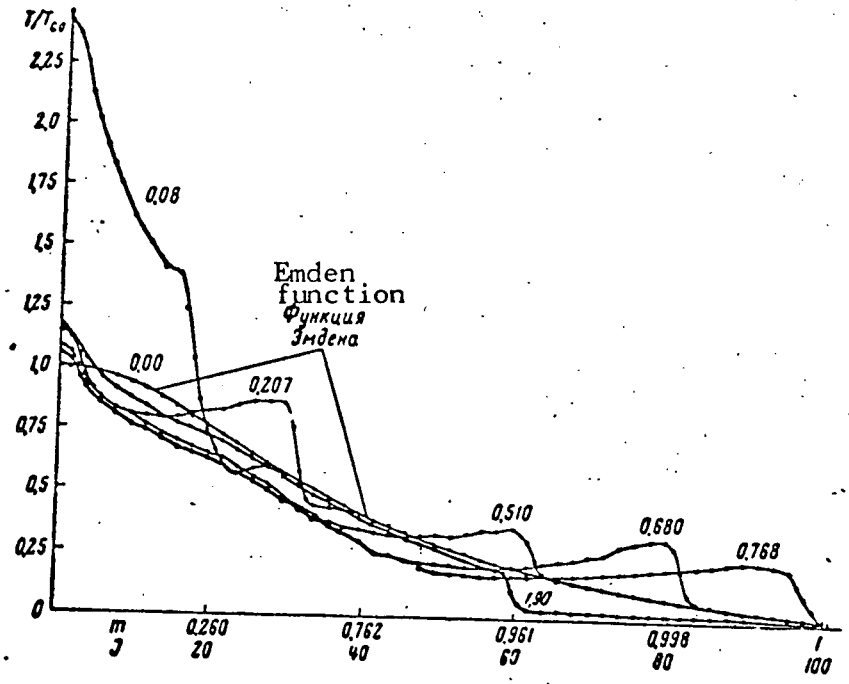

Figure 2. Distribution of temperature after the Lagrangian coordinate for various times (n = 3 b = 1; m_1 = 0.276).

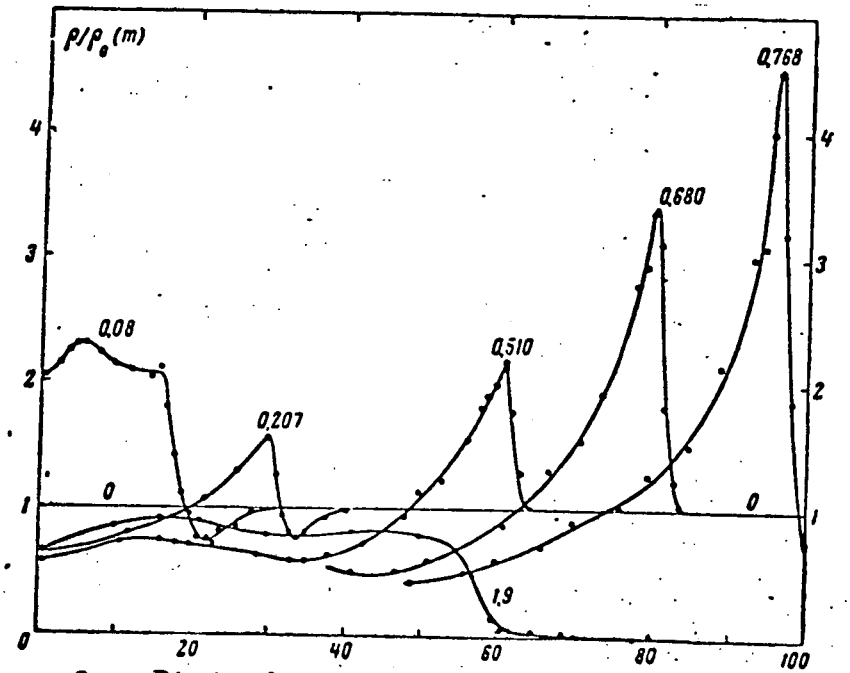

Figure 3. Distribution of density after the Lagrangian coordinate for various times (n = 3; b = -1; m_1 = 0.276. The equilibrium density $\rho_0(m)$ is determined from equations (b)

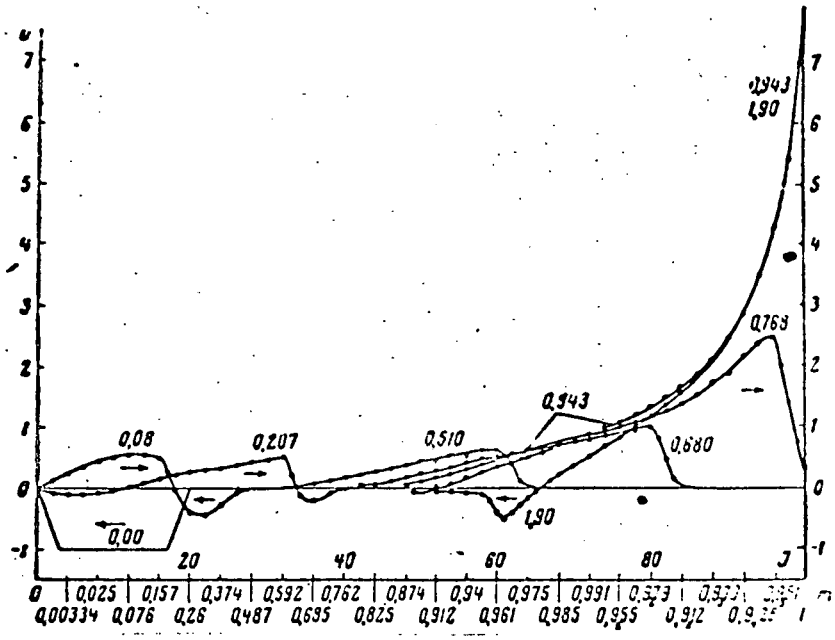

Reproduced from best available copy.

Figure 4. The effect of the Lagrangian coordinate on velocity for various times (n = 3; b = -1; m_1 = 0.276)

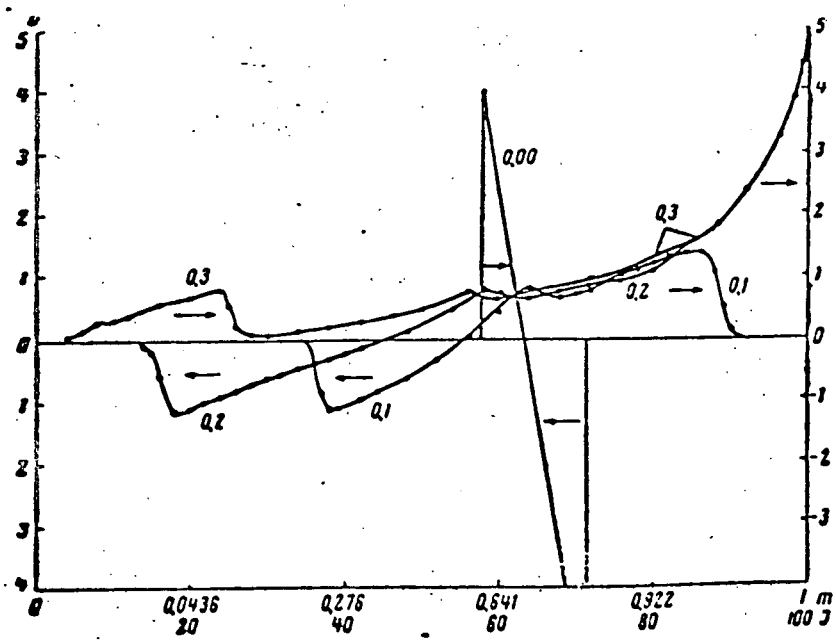

Figure 5. The effect of the Lagrangian coordinate at under surface explosion on velocity for various times (n = 1.5; b = + 4)

Figure 3 shows that at the entrance of the shock wave into the most external layers (t = 0768), the density ratio of its frontal and before the front parts begins to exceed $(\gamma + 1)/(\gamma - 1) = 4$, value indicating a marked effect of radiation pressure. The external layers are expanding with high velocity gradients (the velocity decreases towards the centre) after the emergence of the shock wave at the surface (figure 4). A radius of the star begins to increase rapidly.

The duration of motion of a shock wave from centre to surface is a function of the wave intensity and varies from 0.3 for the strongest perturbations, where the star is completely disintegrated, to 1.6 for the weakest perturbations as given in tables 1 and 2.

The motion of gas for the off-center explosions are shown in figure 5. After a time interval equal to 0.1, we have two shock waves diverging from a locus of explosion, instead of two collapsing gas masses. Once again after 0.1 interval, one of the waves is reaching the surface whereas the second one continues to advance toward the center; then it is reflected from the centre and begins its motion toward the surface.

Thus a picture may be visualized by assuming that after an undersurface explosion a less intensive

central explosion takes place after some time interval. The qualitative description of shock waves from undersurface explosions is given in (8, 9). The equation of hydrostatic equilibrium is disturbed at cooling of the centre and the cooled gas begins to move toward the center, the shock wave is formed which, after some time interval, is reflected from the centre and its subsequent propagation does not differ from the previous cases.

§5. ENVELOPE EJECTION

As it was shown in the previous paragraph, the surface layers of the star acquire some velocity monotonically decreasing toward the star center at the arrival of the shock wave on the surface. Our results are in a good agreement with an automodel problem solution of the arrival of shock waves at the star surface (10). For the final entrance stage of shock wave the asymptotic distributions of velocity, density and pressure were obtained in (10). The velocity, for example, decreases according to the exponential law with an increase in depth.

If the initial perturbation is strong enough, so the velocity of the extreme external layers is greater than the local parabolic one. In so far as the velocity is monotonically increasing toward the surface, so all the layers with velocities greater than the parabolic ones cannot be retained by any means and must irrevocably go into the cosmic space.

Table 1

$n = 3$

b	m_1	E	E_K^{env}	E_g^{env}	Δm	R_j	u_j	t_{tap}	t_K	Remarks
−4	0,276	1,66	0,790	1,50	1,00	296	23,3	0,32	12,0	Complete scattering
−3	0,276	0,933	0,250	0,352	0,203	208	18,5	0,40	10,7	Supernovae
−2	0,276	0,415	$4,86 \cdot 10^{-2}$	$6,88 \cdot 10^{-2}$	$4,62 \cdot 10^{-2}$	121	13,1	0,52	9,0	Novae near the center collapse
−1	0,276	0,104	$2,54 \cdot 10^{-2}$	$4,03 \cdot 10^{-2}$	$3,33 \cdot 10^{-2}$	116	7,68	0,77	14,7	
−0,5	0,276	$2,59 \cdot 10^{-2}$	$1,77 \cdot 10^{-4}$	$2,87 \cdot 10^{-4}$	$2,59 \cdot 10^{-4}$	21,5	4,72	1,01	5,0	
−0,3	0,276	$9,33 \cdot 10^{-3}$	$2,62 \cdot 10^{-5}$	$4,84 \cdot 10^{-5}$	$4,51 \cdot 10^{-5}$	31,9	3,58	1,15	9,0	
−0,1	0,276	$1,04 \cdot 10^{-2}$	$5,28 \cdot 10^{-7}$	$1,20 \cdot 10^{-6}$	$1,17 \cdot 10^{-6}$	9,8	1,95	1,30	5,3	
—	0,32	−0,284	$8,45 \cdot 10^{-4}$	$1,01 \cdot 10^{-3}$	$8,79 \cdot 10^{-4}$	10,5	6,2	0,95	2,5	Centre cooling
—	0,32	−0,116	$2,99 \cdot 10^{-5}$	$7,80 \cdot 10^{-5}$	$6,81 \cdot 10^{-5}$	—	5,4	1,6	6,6	

Table 2

$n = 1{,}5$

b	m_1	E	E_K^{env}	E_g^{env}	Δm	R_j	u_j	t_{tap}	t_K	Remarks
−3,0	0,276	1,11	0,651	0,857	1,00	41,0	5,14	0,35	7,8	Complete scattering
−2,7	0,276	0,898	0,460	0,857	1,00	98,1	4,86	0,44	18,8	Complete scattering
−2,0	0,276	0,492	0,107	0,225	0,199	126	4,20	0,55	28,0	Supernovae
−0,55	0,276	$3{,}70\cdot10^{-2}$	$2{,}9\cdot10^{-5}$	$1{,}5\cdot10^{-4}$	$1{,}44\cdot10^{-4}$	28,4	1,02	—	9,50	
−3,5	0,0436	0,201	$0{,}982\cdot10^{-2}$	$2{,}13\cdot10^{-2}$	$1{,}90\cdot10^{-2}$	35,1	2,79	0,64	11,7	
−2,5	0,0436	0,103	$1{,}02\cdot10^{-3}$	$2{,}75\cdot10^{-3}$	$2{,}51\cdot10^{-3}$	18,7	1,86	0,84	9,10	Novae Point Explosion
−2,0	0,0436	$6{,}58\cdot10^{-2}$	$2{,}88\cdot10^{-4}$	$7{,}90\cdot10^{-4}$	$7{,}85\cdot10^{-4}$	31,1	1,44	0,92	18,5	Novae Point Explosion
−1,5	0,0436	$3{,}70\cdot10^{-2}$	$3{,}42\cdot10^{-5}$	$8{,}8\cdot10^{-5}$	$8{,}78\cdot10^{-5}$	8,4	0,924	1,15	7,0	Novae Point Explosion
−1,4	0,0436	$3{,}22\cdot10^{-2}$	$5{,}3\cdot10^{-6}$	$3{,}15\cdot10^{-5}$	$3{,}15\cdot10^{-5}$	10,2	0,653	1,30	10,0	Novae Point Explosion
+1,4	—	0,898	0,411	0,857	1,00	94,8	5,03	0,20	17,8	Under surface explosion
+2	—	0,225	$4{,}43\cdot10^{-3}$	$8{,}5\cdot10^{-3}$	$8{,}35\cdot10^{-3}$	19,5	2,80	0,30	6,80	$m_0 = 0{,}586$; $m_1 = 0{,}694$; $m_2 = 0{,}818$

Reproduced from best available copy.

into the cosmic space. The machine was automatically able to find a point where the rate of expansion is as equal to the local parabolic one and using the linear interpolation between two adjacent Lagrangian coordinates was able to determine a fraction of the ejected mass Δm, and also, the kinetic energy of this mass taking a numerical integral

$$E_{\text{к}}^{\text{об}} = \frac{1}{2} \int_{\Delta m} u^2 \, dm. \qquad (8)$$

A fraction of the ejected mass Δm sharply increases from zero to some limiting value and then stays constant (figure 6). This mass exactly is the mass ejected into the interstellar space. The kinetic energy of the thrown out envelope (figure 6) and the speed in its external parts (figure 9) conduct themselves in the same manner. After a considerable time interval ($t \approx 10$) we have an envelope expanding with an almost constant rate but sharply variable from its external to internal rims. The envelope goes into a stage of free disintegration where the distance of each Lagrangian layer from the star centre is proportional to the time and the density of each layer is inversely proportional to the cube of the time.

The ejection of an envelope is given in figure 7 in r and t coordinates. The speed of gas on aa' line

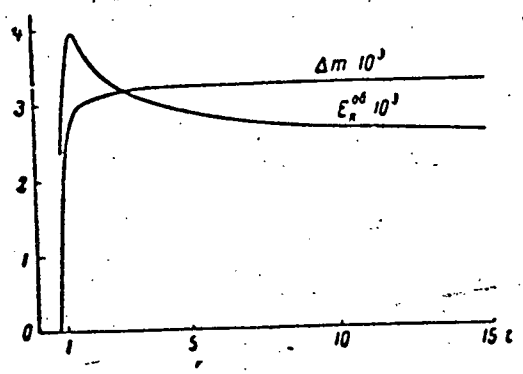

Figure 6. Kinetic energy and envelope mass as a function of time (n = 3; b = -1; m_1 = 0.276)

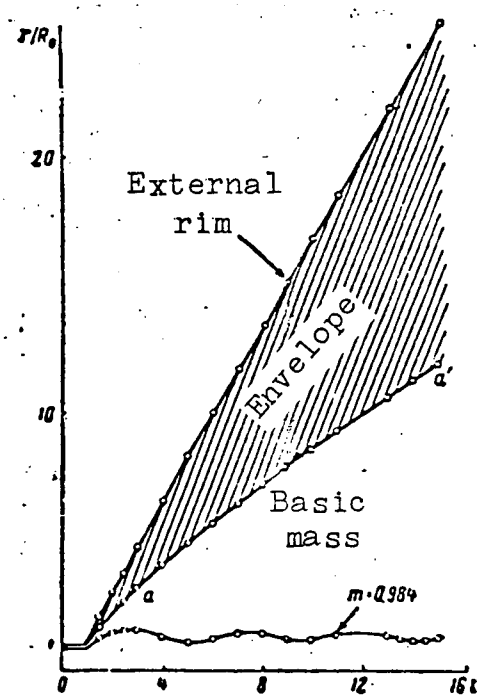

Figure 7. Envelope ejection (n = 1.5; b = - 2.0; m_1 = 0.0436)

is equal to the local parabolic one. Everything located above aa' cannot fall back on the star. The layers located directly under aa' line are receding from the star with a diminishing speed with respect to time. The lower is their positions, the faster their motions are damped and the reverse motion begins. Figure 7 gives the trajectory of a point with the Lagrangian coordinate j = 90 (m = 0.984). This point and also, the points nearest to the star centre are already in a state of oscillatory motion.

Figure 8 shows the effect of a Lagrangian coordinate on the radius. The star forms a very extended envelope whereas the principal star mass is only slightly expanding.

Figure 10 gives the distribution of density in an envelope as a function of r. The density monotionically decreases in the direction of the upper envelope boundary. Thus, an adiabatic approximation does not give an envelope as the spherical layer ejected from the star since the density of external layers decreases faster than the density of internal ones on account of high-velocity gradients.

The closely connected problems of the final envelope separation and the transformation of a premaximum spectrum into the principal one can only be solved by using more detailed calculations and taking the heat conductivity into consideration; it is probable that the corpuscular

radiation (11, 12) plays a very important role in this case.

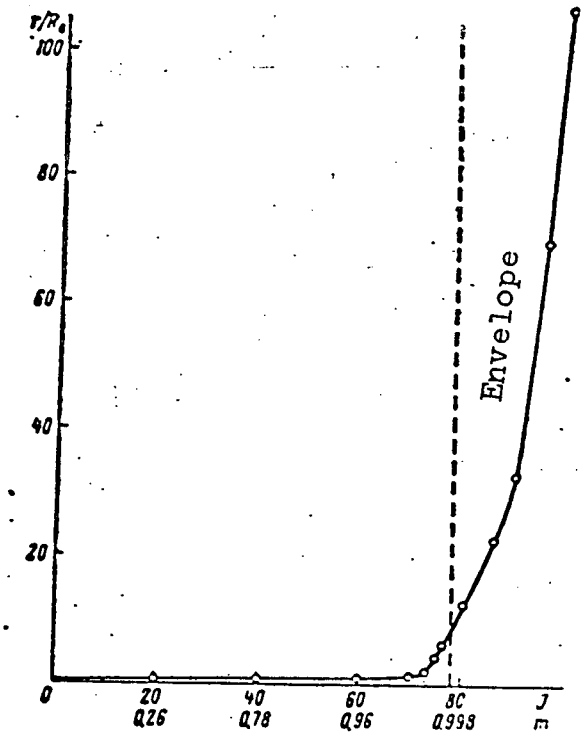

Figure 8. The effect of the Lagrangian coordinate on the radius ($n = 3$; $b = -1$; $m_1 = 0.276$; $t = 14.7$)

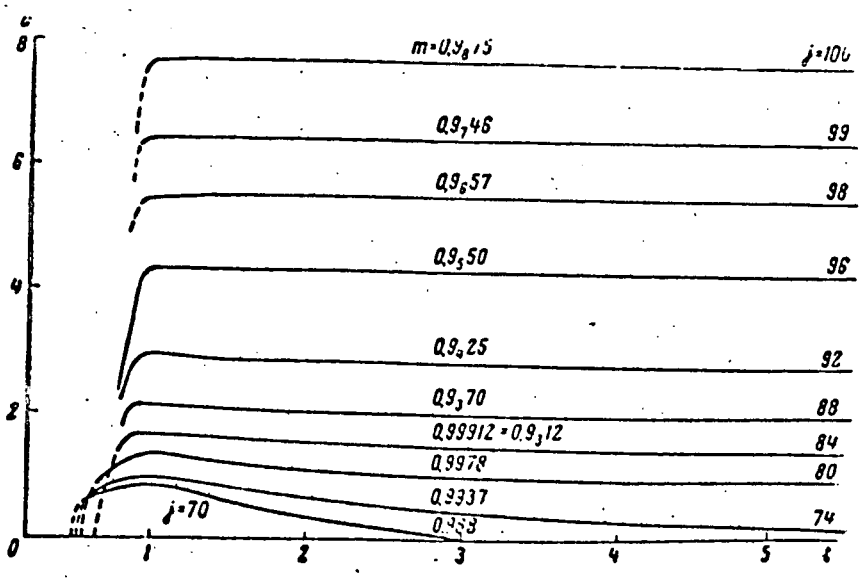

Figure 9. Speed in the envelope as a function of time for various Lagrangian coordinates ($n = 3$; $b = 1$; $m_1 = 0.276$. The envelope boundary is determined by a Lagrangian coordinate $j \approx 78$ ($m = 0.99667$)

Table 1 and 2 give the following characteristics: b, the perturbation amplitude; m_1 the fraction of perturbed mass; E, the total perturbation energy; E_k^{env} - kenetic energy; E_s^{env} - the envelope seperation energy equal to the envelope gravitational energy at the equilibrium postion with a reserved sign; Δ_m - the fraction of ejected mass; R_j - the radius of envelope external rim expressed as the fraction of a balanced radius; U_j - the velocity of the envelope external rim; t_{ap} - the time appearance of a shock wave at the surface; and t_k is the

time when the counting has been discontinued and to which all the values are related.

In a case of centre cooling, the perturbation energy is assumed to be the difference between the total energies of cooled and balanced models, i.e., the amount of heat taken from the balanced model with a reversed sign.

A layer with a Lagrangian coordinate j = 100 is designated as the external layer while the actual vacuum boundary corresponds to j = 100.5. The mass located over the star external rim is 9×10^{-6} and 2.5×10^{-9} of the total star mass for n = 1.5 and n = 3.0, respectively. Figure 13 gives on a logarithmic scale a relationship between the envelope kinetic energy and its mass on the basis of data given in tables 1 and 2.

For relatively weak perturbations, where the envelope mass does not excees $\approx 0{,}3$ of the star mass, this relationship can be approximated by a straight line, with a slope coefficient independent of polytropic indixes.

$$\lg E_{\kappa}^{\text{env}} = 1{,}07 \lg \Delta m + \alpha(n) \quad (10^{-6} \leqslant \Delta m \leqslant 0{,}3), \qquad (9)$$

where

$$\alpha(n) = \begin{cases} -0{,}24, & n = 1{,}5; \\ +0{,}12, & n = 3{,}0. \end{cases}$$

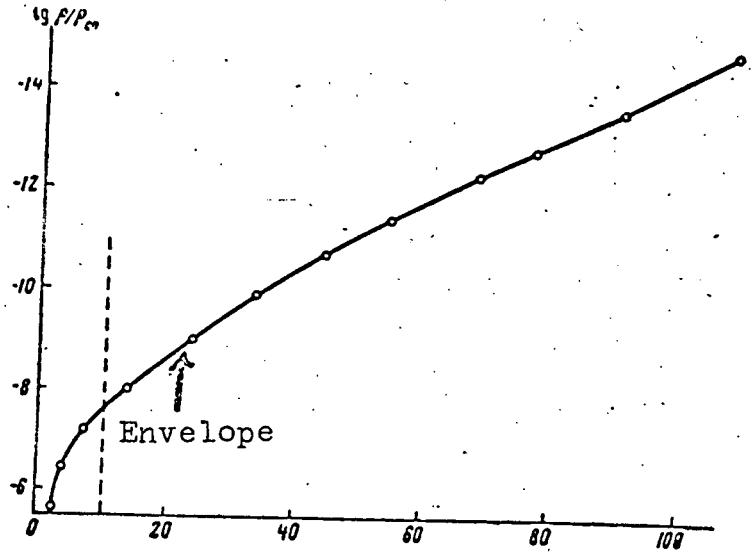

Figure 10. Envelope density as a function of the centre distances (n = 3; b = -1; m = 0.276; t = 14.7)

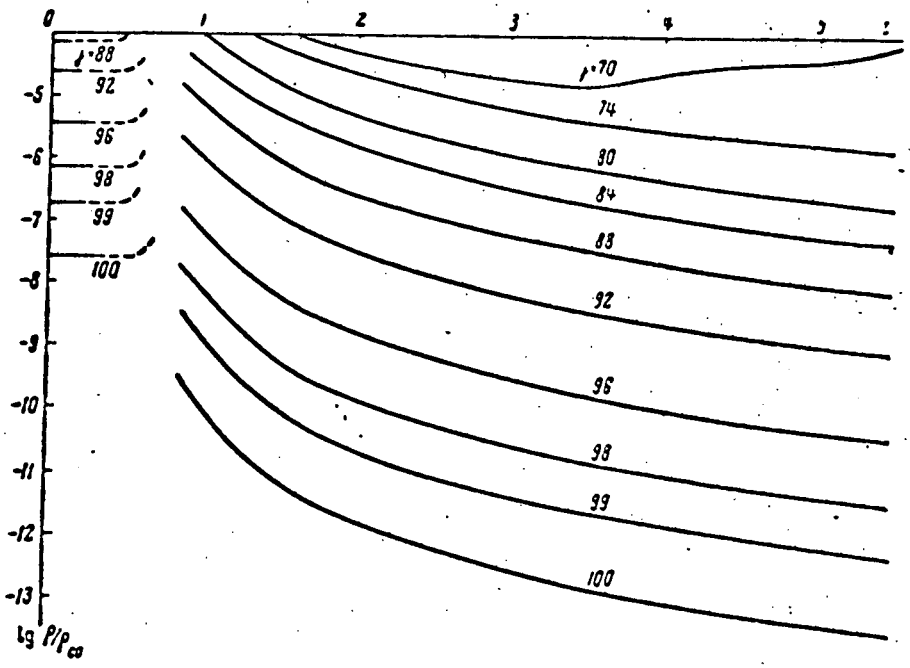

Figure 11. Envelope densities as a function of time for various Lagrangian coordinates (n = 3; b = -1; m_1 = 0.276)

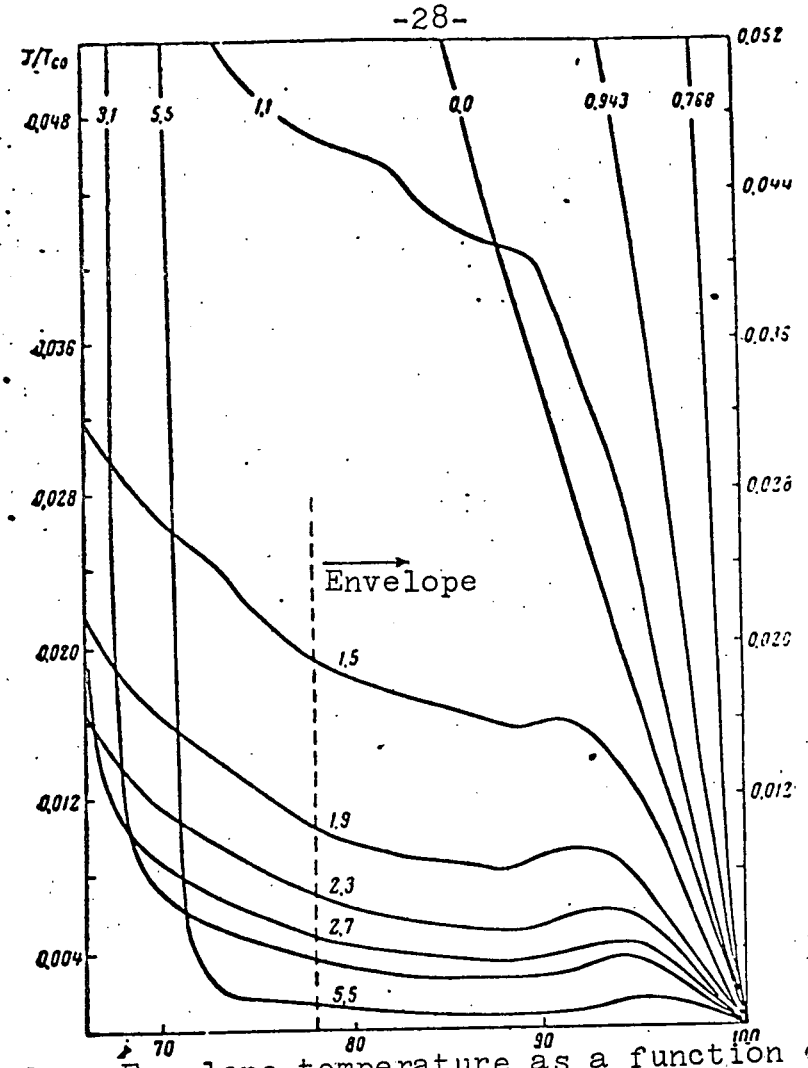

Figure 12. Envelope temperature as a function of the Langrangian coordinate for various times ($n = 3$; $b = -1$; $m_1 = 0.276$)

It is most convenient to introduce the mean envelope velocity which is determined by a relationship:

$$E_{\text{к}}^{\text{env}} = \frac{1}{2}\Delta m\bar{u}^2 \text{ или } \bar{u}^2 = \frac{1}{\Delta m}\int_{\Delta m} u^2\,dm. \qquad (10)$$

By substituting (10) into (9) equation we obtain:

$$\lg \bar{u} = 0{,}035 \lg \Delta m + \varepsilon(n), \qquad (11)$$

where

$$\varepsilon(n) = \begin{cases} 0{,}03, & n = 1{,}5; \\ 0{,}21, & n = 3{,}0. \end{cases}$$

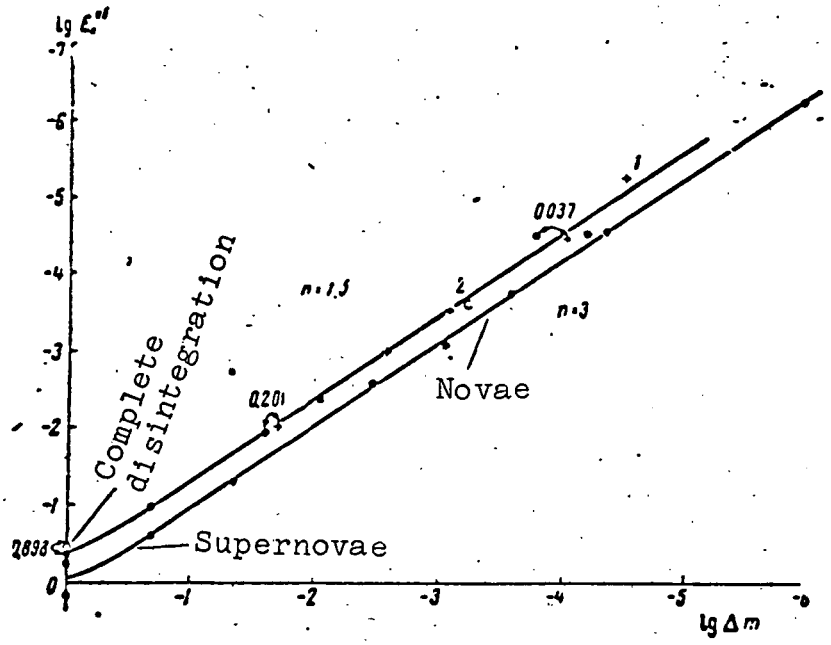

Figure 13. Envelope kinetic energy its mass relationship for various n and various perturbations

(11) shows that the dimensionless mean velocity almost does not depend on the fraction of ejected mass or what is the same thing, on the force of perturbation and only depends on a polytropic index.

In order to evaluate the effect of the form of perturbation on (9) and (10) relationships, the various variants marked on figure 13 as points, crosses, triangles, and stars were checked.

The points correspond to a central perturbation with a perturbed mass $m_1 = 0.276$(figure 10), the crosses also correspond to a central perturbation but with a perturbed mass $m_1 = 0.0436$ (a model of point explosion), the triangles belong to an undersurface explosion, and the stars correspond to centre cooling. Points 1 and 2 are only distinguished by their signs of amplitude perturbation b. In both of these cases the central perturbation has the same form and energy, but in the second case the "collapse" with the subsequent reflection from the centre took no place, and all the points of perturbation region have immediately acquired a velocity directed from the centre.

The points with equal perturbation energies and with different perturbation masses are connected with brackets with perturbation energy values given above them.

All these points practically are located along one straight line and small deviations for n = 1.5 and

log $\Delta m < -4$ can be explained by the errors in the evaluation of an integral of the envelope kinetic energy (8), since in this case the envelope only has 3 - 4 calculated invervals. For a polytropic index n = 3, the envelope contains considerably more computed points and here weaker explosions can be evaluated.

Figure 13 shows that the kinetic energy - envelope mass relationship slightly depends on the method of formation of a shock wave and basically on a polytropic index.

Thus, we have obtained reasonably reliable basic envelope characteristics: mass, velocity, and kinetic energy. In regard to such important properties as brightness and effective temperature, we are not able to investigate them in the present computation basically for two reasons:

1. The adiabatic approximation is well realized at the propagation of shock waves within the star. Shortly after the formation of a shock wave a heat-conductivity term in a system of equations (3) begins to play a significant role and we have no justification for applying the adiabatic approximation to the envelope.

2. At relatively small ejected masses ($\Delta m \leqslant 10^{-2}$) the envelope contains from 4 - 20 computed points, that is clearly not sufficient for the evaluation of detailed structure.

§6. THE MOTION OF THE PRINCIPAL STAR MASS

Four cases of total star ($\Delta m = 1{,}00$) disintegration are given in tables 1 and 2. The total disintegration takes place when the perturbation energy is equal to the gravitational star energy with a riversed sign. If the perturbation energy does not exceed, in its absolute value, the gravitational star energy, so the star disintegration is not complete. The total disintegration also does not take place in cases where the total energy of perturbed model is positive, and here the excess of energy is carried away by the envelope as its kinetic energy and as the separation energy. The remaining star mass now possesses the negative total energy. In all four variants of total disintegration (tables 1 and 2) the perturbation energy somewhat exceeds the gravitational one which for a polytropic index n in dimensionless units is equal to:

$$E_g = -\frac{3}{5-n} = \begin{cases} -1{,}5, & n = 3; \\ -0{,}857, & n = 1{,}5. \end{cases}$$

At total disintegration, a region of decreased density is formed near the centre and at some distance from it the density is reaching its maximum value, and then sharply decreases with an increase in distance from the centre. The internal star energy is sharply decreasing

with time, the gravitational energy tends to zero, and the kinetic energy tends to a constant value which is equal, according to the law of conservation of energy, to the sum of energies of a balanced star and perturbation.

At undersurface explosions, the total disintegration also takes place when there is the equality between the absolute energies of gravitation and perturbation. The final disintegration takes place after the reflection of the second shock wave from the centre. (See figure 5).

Figure 14 shows the changes, with respect to time, of the gravitational and internal energies of the total star. We see that after the arrival of a shock wave at the surface, the principal star mass forms damped oscillations. The oscillations are damped with respect to a new state of equilibrium with large total energy. For a new state of equilibrium the ratio of gravitational to internal energies is exactly equal 2, as it should be after the virial theorem. The structure of a star in its new equilibrium state does not significantly deviates from a polytrop n = 3 with an exception of region near the center $(m \lesssim 0{,}2)$ and the most external layers. Some time after an explosion we have the principal star mass in its new equilibrium position and the envelope receding from the star with constant velocity. A period of

pulsation of principal mass in dimensionless unit is equal

$$P_0 = \begin{cases} 2{,}1, & n = 3; \\ 4{,}6, & n = 1{,}5. \end{cases} \qquad (12)$$

A pulsation constant is introduced into the theory of star pulsation as follows:

$$Q = P\sqrt{\bar{\rho}/\bar{\rho}_\odot}; \qquad (13)$$

where ρ and $\rho_\odot$ are the mean densities of a star under investigations and the sun, respectively, and P is the period of pulsation expressed in days. If P is expressed in our dimensionless units and instead of the mean density we substitute its value $\bar{\rho} = \frac{3M_0}{4\pi R_0^3}$, we have

$$Q = t_\odot P_0, \qquad (14)$$

where $t_\odot = \left(\frac{4\pi}{3} G\bar{\rho}_\odot\right)^{-\frac{1}{2}} = 0.01845$ days.

The values of pulsation constants under the condition of a small oscillation amplitude are evaluated for various star models.

Thus, for the polytrops (principal mode) (13)

$$Q = \begin{cases} 0{,}0703, & n = 1{,}5; \\ 0{,}0383, & n = 3{,}0. \end{cases} \qquad (15)$$

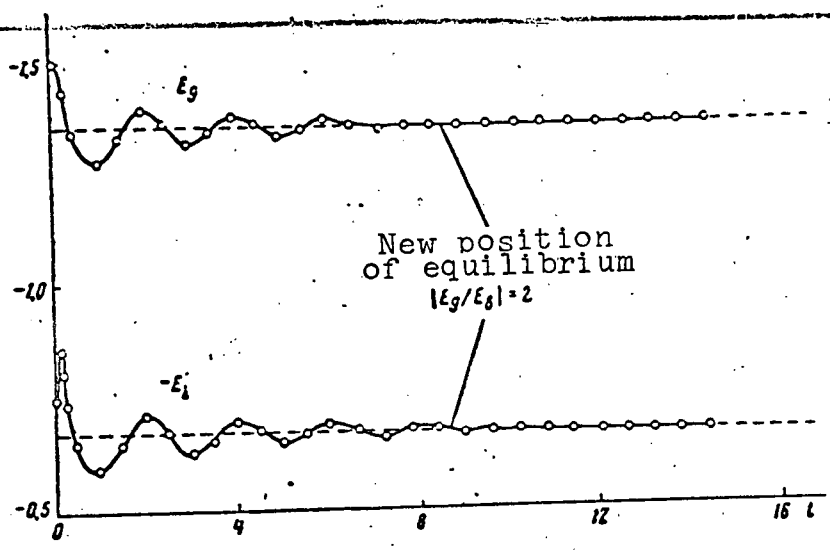

Figure 14. Internal and gravitational energies of the whole star as a function of time (n = 3; b = -1; m_1 = 0.276)

By substituting equation (12) into equation 14, we obtain:

$$Q = \begin{cases} 0{,}0850, & n = 1{,}5; \\ 0{,}0388, & n = 3{,}0. \end{cases} \qquad (16)$$

The values of pulsation constants (16) well agree with the computed values using the linear theory of pulsation (15). Thus a star after explosion pulsates in its principal mode. Somewhat higher values of the pulsation constants can be explained by the presence of non linear pulsations.

Let us investigate the motion of a gas directly at the envelope lower boundary with its velocity smaller than the parabolic one. Under the action of the force of gravity the gas begins its reverse motion toward the star center and, colliding with deeper layers, forms the shock front which with time slowly moves to the boundary of expanding envelope; this front is well visible in figures 3 and 4 (t = 1.9) and in figure 12 (t = 3.1; 5.5).

Since for large time intervals heat conductivity begins to play a significant role, so the final fate of this front, as well as the evolution of the whole process under study, should be studied by taking into consideration the transfer of radiation energy without using the adiabatic approximation.

§7. DISCUSSION OF THE RESULTS FROM THE VIEW POINT OF OBSERVATIONS

It is necessary to use dimensional units in order of comparing with the observations. If the mass and radius of a star in equilibrium are expressed through the sun parameters, so we obtain from equation (2) the following expressions for the unit of time, speed, and energy:

$$\left.\begin{aligned} t_0 &= 0{,}01845\,(R_0^3/M_0)^{1/2}\ \text{сут};\\ u_0 &= 436{,}8\,(M_0/R_0)^{1/2}\ \text{км/сек};\\ E_0 &= 3{,}797\cdot 10^{18}\,M_0^2/R_0\ \text{эрг}. \end{aligned}\right\} \qquad (17)$$

The dimensionless values used by us are equal to the dimensional ones divided by its corresponding dimensional unit (17). By taking this into consideration, we obtain from (11) the relationships between the dimensional values as follows:

$$\lg \bar{u} = 0{,}465 \lg M_0 + 0{,}035 \lg \Delta M_0 - 0{,}5 \lg R_0 + \sigma(n); \qquad (18)$$

$$\sigma(n) = \begin{cases} -0{,}33, & n = 1{,}5; \\ -0{,}15, & n = 3{,}0. \end{cases}$$

Here M_0 and R_0 and also, an envelope mass ΔM_0 are expressed in the solar units and the speed in thousands of KM/s.

The observed parameters of Novae stars are: the mass of an ejected envelope, its speed, and also its radius prior to the burst, however, the masses of the Novae stars up to now remain an unknown link. At present we only have an evaluation of the mass of NHer 1934 (14, 15), Novae star. Therefore it is natural to apply formula (18) for the determination of the Novae masses and in this connection the Nova radius R_0 prior to the burst, the mass of ejected envelope ΔM_0 and the mean envelope speed must be known from the observation data.

Formula (18) is used in an investigation (16) for the evaluation of masses of the ten best known Novaes.

The masses of fast Novae, of NAql 1918 type, were estimated as equal several sun masses and the masses of slow Novae, of NHer 1934 and NAurl 891types, considerably smaller, i.e., $0.2 \div 0.02\ M_{\odot}$. At bursts, the Novae eject an insignificant fraction of their mass, of the order of $10^{-4} \div 10^{-5}$ (16).

The interpolation formula (18) also is correct, where the fraction of ejected mass is 0.1 - 0.3; this corresponds to the bursts of Supernovae.

Unfortunately the paucity of observations pertaining to the Supernovae does not permit the evaluation of their masses.

Some numerical data of interest are discussed here. Assume that prior to its burst the Novae has a polytropic structure with $n = 3$, $R_o = R_{\odot}$, and $M_o = 3M_o$ (fast Novaes (16)). Then, according to (17), a time unit is 0.011 day = 0.26 h and the time of propagation of a shock wave from the centre to the surface is of 0.26 h order and the pulsation period after the explosion will be equal to 0.55h. The photosphere radius of Novaes at their maximum brightness is about 100 $R_{\odot}$ (17). We obtain from tables 1 and 2 that the radius of the envelope external rim of the Novaes attains this value for $t = 30 \div 50$. In dimensional units, the time of growth of brightness from its minimum to maximum values is, thus, 10h.,

approximately. This gives the lower value since the radius of a photosphere should be increased more slowly than the radius of the envelope external rim on account of the translucence of external layers.

Our model will have central temperature approximately equal $T_{co} = 60 \times 10^6$ °K (for a molecular weight $\mu \approx 1$) Figure 3 shows that the temperature jump of the shock-wave front in its passage into the surface layers is $\approx 0,2\, T_{co}$ or 12×10^6 °K. Shock waves are responsible for a strong heating of surface layers.

CONCLUSION

The given computations give the preliminary mechanical model of the Novae bursts. The neglect of heat conductivity and incomplete ionization of external layers, the assumption of spherical symmetry, the uncertainties pertaining to the structure of the Novae, and the generation of shock waves, all this renders the computations only to be a weak step to the quantitative study of this most interesting phenomenon.

We express our deepest thanks to V.S. Imshennik and R.P. Fedorenko without whose support and valuable help this investigation would be hardly possible; also Ya. B. Zel'dovich, S.B. Pikel'ner, M.S. Frolov, and I.G. Kolesnik for their interest in this investigation.

REFERENCES

1. Hazlehurs, J. Advances in Astronomy and Astrophysics, 1, 1 Acad. Press. New York - London 1962.

2. Ono Yôrô; Sakashita Shirô; Ohyama Noboru, Suppl. Progr. Theoret. Phys., 1961, N 20, 85.

3. Chandrasekar, S. Introduction into the study of star structure (Vredenie V Ychenie o stroenii zvezd) IL, 1950.

4. Heney J.G.; L. Wilets; K.H. Böhm, A.O. Astrophys J 1959, 129, 628.

5. Rikhtnayer, R.D. Different methods for the solution of rim problems, IL, 1960.

6. Berezin, I.S.; N.P. Zhidkov, Computation methods (Metody tvychisleniy) v.2, M. Fizmatgiz, 1960.

7. Mathematical Tables of British Assoc. of the Advances in Science, 2, London, 1937.

8. Lebedinskiy, A.I., Astr. Zh. 1952, 29, 135.

9. Gurevich, L.E., A.I. Lebedinskiy, Transactions of the 4th Congress on the problem of cosmogony (Trudy chetvertogo coveshchaniya po voprosam kosmogonii) Izd-vo ANSSSR, 1955, pp. 165 - 171.

10. Gandel'man, G.M., D.A. Frank-Kamenetskiy, Report of ANSSSR, (Dkl. ANSSSR) 1956, 107, 811.

11. Mustel, E.R., Astr. Zh. 1962, 39, V.2, 185.

12. Garbatskiy V.G. Astr. Zh. 1962, 39, V.2, 198.

13. Ledoux, P.; H. Walraven, Handbuch der physik, 51, Berlin - Springer, 1958, S. 473.

14. Kraft, R.P., Astrophys J., 1959, 30, 110.

15. Walker, M.F., Astrophys J., 1956, 123, 68.

16. Nadezhin, D.K.; D.A. Frank-Kamenetskiy, Astrophys Zh., 1962, V. 6, 1003.

17. Payne-Kaposhkin, S.; Handbuch der Physik, 51, Berlin-Springer, 1958, S. 752.

FIGURE 4

GENERAL AVIATION RANGE ALTITUDE CAS THREAT LOGIC

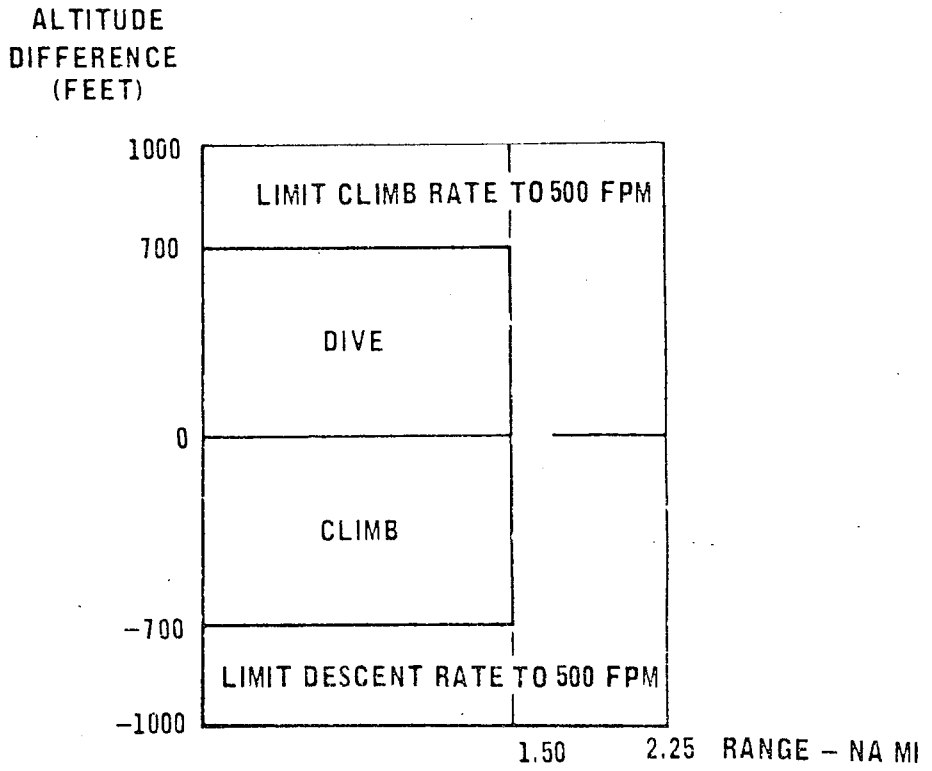

The logic first checks the measured differential altitude to determine if the intruding aircraft is in the co-altitude band or outer altitude band. If the magnitude of the differential altitude is less than the threshold value of the outer altitude band, the logic next determines from the measured range which alarm zone applies. Depending upon the particular zone and altitude band, the cockpit indicator command is determined by the logic as shown in the figure.

For the case of an intruding aircraft entering the threat zone through the top or bottom, the outer altitude band must be located so that the aircraft will have reduced their altitude rates before entering the inner altitude band. The inner altitude band is located, so that there is a high probability of having more than the minimum safe altitude separation as horizontal range separation approaches zero.

In a General Aviation versus Commercial Aviation encounter, the Commercial Aviation aircraft must initiate the escape maneuver (e.g., a range warning of 1.5 nautical miles would not be adequate if a General Aviation aircraft were to be soley responsible for providing 100% protection).
The MICRO-CAS transmissions, when received by a Commercial CAS, are processed the same as another Commercial CAS transmission (Doppler is measured). Thus, the commercial aircraft will have the required full warning time to make the necessary collision avoidance maneuver. The General Aviation collision avoidance logic is designed primarily for the General Aviation versus General Aviation encounter.

The MICRO-CAS depends on resync from either a ground station or an airline aircraft. Fortunately, the airlines have agreed to provide air to air synchronization in their equipment.

HARDWARE

The MICRO-CAS is packaged in a standard double panel width General Aviation instrument case (12" x 6 1/2" x 3 1/2") as shown in Figure 5. The pilot indicator and control unit is self-contained when the main case is instrument panel mounted. When the main case must be remotely located, the indicator and control unit may be detached and mounted on the instrument panel separately. The weight of the main case with indicator and control unit contained is approximately eight pounds. The input power required is approximately 3 amperes at 13.75 Volts.

FIGURE 5

MICRO-CAS

Reproduced from best available copy.

Figure 6 depicts the major components of MICRO-CAS. The functions of the various components are:

- o Circulator/Limiter - Protects receiver during transmission periods.
- o Receiver - Receives and demodulates range, altitude, and resync data from other CAS stations.
- o Threat and Resync Logic - Computes existence of a threat and commands appropriate maneuver on the display, and controls synchronization and timing.
- o Display - Provides visual maneuver command and accompanying audio alert.
- o Oscillator - Provides basic frequency to drive the system, keeps MICRO-CAS time aligned with CAS time reference.
- o Modulator/Encoder - Encodes altitude and activates transmitter upon command of resync logic.
- o Transmitter - Broadcasts ranging and altitude signal in own slot.

FIGURE 6

BLOCK DIAGRAM

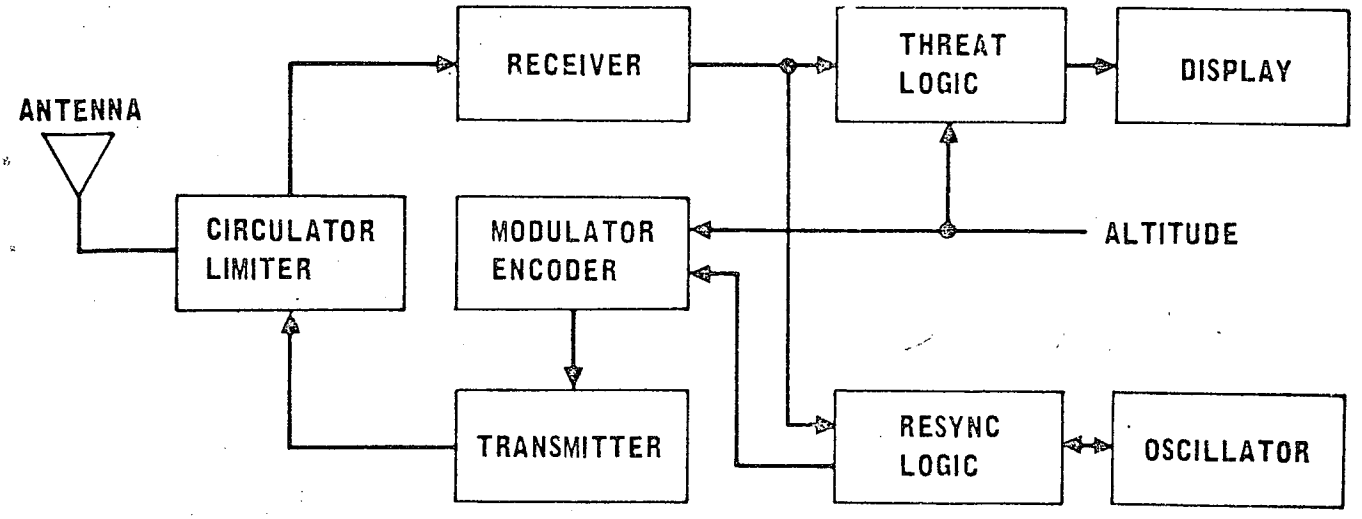

The display for the general aviation MICRO-CAS is a simple, low-cost indicator consisting of on-off lights driven by the CAS logic. It includes both command and advisory information. The commands consist of a beeping audio warning tone coupled with a flashing red symbol, telling the pilot to climb, dive, or hold altitude to avoid collision.

Advisory information is provided by lighting the upper half of the indicator in yellow with the words LIMIT CLIMB TO 500 FPM, if an aircraft above could become a collision threat with altitude and/or range closure. The lower half of the display is illuminated in yellow with the words LIMIT DESCENT TO 500 FPM, if an aircraft below could become a collision threat. These yellow advisories are not commands, but place restrictions on the pilot's vertical maneuvering if he wishes to minimize entering a potential collision situation. If he does not heed these restrictions, he will receive a red command when his range to the other aircraft reduces to 1.5 n.m and his altitude difference is reduced to 700 feet.

While the aircraft is on the ground, the "STDBY" button should be depressed. An amber light will indicate the system is receiving power, but is not transmitting an altitude signal. This is to prevent giving a false warning to other airborne aircraft approaching the terminal. Shortly after take-off, the pilot should depress the "ON" button to make the CAS function completely. If the system is synchronized and functioning normally, the "ON" button will be illuminated green. On aircraft with retractable landing gear, these functions may be handled automatically by a switch activated by the retraction of the landing gear. However, the amber and green lights will still indicate the status of the system. If the "ON" button has been activated and the green light does not illuminate, the system has not

completed warm-up time or is not within communication range of a synchronization donor. Thus, to have CAS protection, the green light must be on.

REFERENCES

1. "Airborne Collision Avoidance System" issued by the Air Navigation/Traffic Control Division, Air Transport Association of America, ANTC Report No. 117, 31 July 1970, Revision 9.

2. "System Study For The Application of Time Reference Techniques to General Aviation For Collision Avoidance", NASA/ERC Contract No: NAS 12-2182, MDC Report No. MDC E0079, 2 March 1970.

Printed by the Department of Transportation - Federal Aviation Administration

37281